

July 19, 1996

A prognostic ice cloud parameterization for GCMs based on modeled and observed behavior of tropical anvils

Charles S. Zender and J. T. Kiehl

National Center for Atmospheric Research, Boulder, Colorado

Abstract. We document the development of a parameterization of cirrus cloud suitable for implementation in general circulation models (GCMs). The parameterization, called ANV (for anvil), comprises convective (sub-gridscale) and stratiform (resolved) condensation. Both components represent the bulk processes of deposition, sublimation, and precipitation of ice mass without assuming or predicting the ice particle size. We employed a cumulus ensemble model (CEM) to determine parameters governing ice generation in the convective case, and a size resolving column model in the stratiform case. As a result ANV predicts the ice budget of a GCM atmospheric column from the convective mass flux, updraft, temperature, humidity, and inferred budgets of observed convective systems. Statistics from control runs of a GCM and the CEM revealed fundamental distinctions in the convective behavior of each model in a tropical convecting regime. Sampling the CEM dataset using convective criteria which minimize systematic differences in the mass flux profile between models permits ANV to be mapped from the high to the low resolution model in a physically consistent manner.

1. Introduction

Ice cloud has a significant impact on the radiative budget of the earth and presents a great challenge to modeling its climate. Ice cloud contributes more than any other cloud type to total continental cloud cover and rank second to marine stratocumulus in tropical oceanic coverage [Warren et al., 1986, 1988]. Deep convection in the tropics generates anvils in the coldest part of the troposphere, over the warmest SST—ideal conditions for trapping longwave emission from the surface. In the tropics, net cloud forcing is a small residual between shortwave and longwave cloud forcing (SWCF and LWCF) whose magnitude largely depends on two properties: cloud mass and height [Kiehl, 1994a]. A small bias in either property can change the sign of feedbacks between cloud forcing, SST, and convection which control the hydrologic cycle. Satellite datasets exist that document the direct influence of cloud on the global energy budget [e.g., Ramanathan et al., 1989], but their role in the hy-

drologic cycle remains largely speculative. Sun and Lindzen [1993] argue that the observed vertical distribution of tropical water vapor can be maintained by sublimating hydrometeors detrained from cirrus. For these reasons, the prediction of ice cloud in a general circulation model (GCM) should include the essential physics that determine tropical anvil vertical and geographic distribution, longevity, and mass.

The treatment of ice cloud by GCMs falls into two classes: diagnostic and prognostic. Diagnostic schemes employ empirical relationships among large scale variables (e.g., temperature and humidity) to obtain the mixing ratio of condensed water q_c [e.g., Kiehl et al., 1996], or a proxy, such as cloud optical depth [Hansen et al., 1983]. Their prescribed, steady state nature makes diagnostic schemes computationally efficient. Typically some form of entraining plume is implicitly assumed, so that the q_c profile increases with height above cloud base more slowly than, but similar to, an adiabatic condensed water

profile.

While variations on it can perform well for entraining plumes, an adiabatic profile is ill-suited as a basis for predicting the vertical distribution of condensate resulting from deep convection. Deep convection is characterized by an active core region much smaller than the associated mesoscale outflow (anvil). The relative area of a core to its anvil is $< 10\%$ [Fu et al., 1990]. Typical anvil depth is 5–10 km (resolvable by current GCMs) [Wong et al., 1993a]. In contrast to the monotonic adiabatic profile, observations and cloud resolving simulations [Wong et al., 1993b; Sui et al., 1994; Grabowski et al., 1995] show the area-averaged vertical q_c profile of a mature (or time-averaged) anvil system varies little (and can increase) from freezing level to ~ 300 mb, above which q_c decreases rapidly. Furthermore, detached anvils can project a radiative influence long after deep convection ceases [Ackerman et al., 1988]. Representing this convective-radiative hysteresis is an important advantage of prognostic over diagnostic schemes. The fidelity of diagnostic schemes could be improved by transmitting information about the synoptic environment to them, but this is a complicated, non-local procedure.

Representing a wide spectrum of cloud types is more naturally accomplished by prognostic schemes, which forecast q_c each timestep with an equation incorporating physically based sources, sinks, and transport. Our interest is the sensitivity of the climate system to tropical anvils. A forecast q_c allows hysteresis, and so can maintain long-lived anvils after the cessation of convection. Prognostic cloud schemes occupy a spectrum from relatively simple, single category bulk condensate treatments [e.g., Sundqvist, 1988], to complex multiple category (droplet, rain, graupel, crystal, snow etc.) treatments that also predict size spectra [e.g., Flatau et al., 1989]. Complex schemes include more physical processes whose details are poorly understood (e.g., homogeneous nucleation) and will remain difficult to test against observations for many years. Prior studies of the effects of cirrus employed either diagnostic cloud schemes [e.g., Slingo and Slingo, 1988; Randall et al., 1989], or prognostic schemes [e.g., Senior and Mitchell, 1993; Sherwood et al., 1994; Fowler and Randall, 1996; Del Genio et al., 1996] that detrain (with a specified, sometimes 100%, efficiency) condensate predicted by a moist convection parameterization into the stratiform anvil. In the latter models, detrained condensate is consistent with the moist convective parameteriza-

tion, but may not include condensate formation from secondary circulations. To our knowledge, only Donner [1993] explicitly accounts for condensate formed by mesoscale circulations outside the deep convective core (perhaps 25–40% of total anvil condensate [Leary and Houze, 1980; Gamache and Houze, 1983]). The main purpose of this study is to develop a prognostic cloud scheme in which deep convection results in the generation and maintenance of mesoscale anvils with realistic q_c profiles and lifetimes.

Previous studies [Slingo, 1987; Sundqvist, 1988; Xu and Krueger, 1991] agree that the total cloud field is best parameterized as the net result of convective and stratiform cloud processes. Long term, multi-regional datasets on cloud microphysics, radiation, and mesoscale dynamical features needed to develop and fully test prognostic ice cloud parameterizations do not exist. In the interim many in the GCM community feel the best tool available for studying deep convection and associated mesoscale outflow is the cloud-resolving cumulus ensemble model (CEM) [Browning, 1994]. Current computational resources allow one to define CEM domains that extend beyond the scale of a typical GCM grid box. Thus, these models serve as a bridge from the cloud scale up to the scale of the GCM. For prognosing stratiform ice associated with large scale ascent and cooling, a size resolving column model (SRCM) may suffice. This study combines results from SRCM, CEM, and GCM simulations with empirical estimates of convective system hydrologic budgets into a parameterization scheme for ice cloud dubbed ANV (for anvil). A second paper [Zender and Kiehl, 1996] describes the sensitivity of the simulated climate of a new version of the National Center for Atmospheric Research Community Climate Model (NCAR CCM) to the radiative effects of the enhanced upper tropospheric ice amount and fraction predicted by ANV.

The paper is organized as follows: Section 2 summarizes the 24 day numerical experiment performed with the CEM. We analyze the CEM dataset and develop the convective component of ANV in Section 3. The technique used to mesh the convective portion of ANV with a GCM in a physically consistent manner is shown in Section 4. Section 5 describes the SRCM and documents the stratiform component of ANV. Section 6 contains concluding remarks.

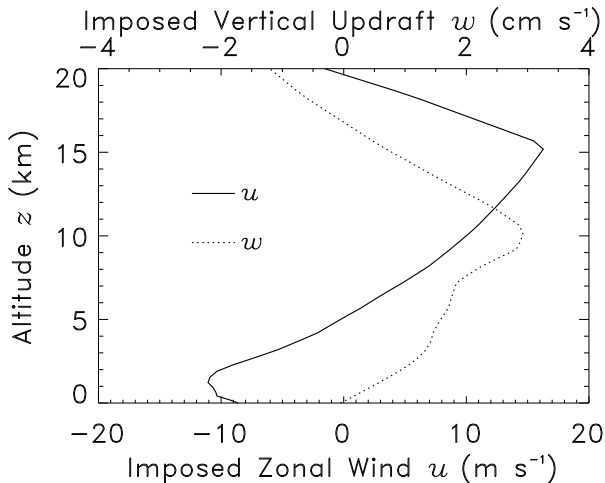


Figure 1. Imposed vertical profiles of large scale forcing in the CEM: Horizontal wind shear (solid) and large scale ascent (dotted).

2. Cumulus Ensemble Model

We employed the CEM developed by Tripoli [1992] for our studies. A more comprehensive review of our CEM simulation is presented by Grabowski et al. [1995]. The model is nonhydrostatic, fully non-Boussinesq and can be run in either a 2-dimensional or 3-dimensional configuration. The model employs a six water category (cloud droplets, rain droplets, pristine ice crystals, snow crystals, aggregates and graupel) bulk formulation for microphysics [Flatau et al., 1989]. The model also includes a parameterization for longwave and shortwave radiation; a turbulent kinetic energy closure; and a Businger-type parameterization for surface exchange. The configuration of the simulations is analogous to the work of Sui et al. [1994]. The model run is 2-dimensional with an outer domain of 900 km and a horizontal resolution of 1 km. The vertical domain extends to 25 km with a variable vertical resolution, with a nominal resolution in the mid-troposphere of 200 m. The horizontal boundary condition is periodic. The model time step is 10 s. A constant surface temperature of 301 °K is assumed to represent Western Pacific conditions.

The model is forced with steady conditions from the Marshall Islands [Yanai et al., 1973]. The imposed zonal wind and vertical updraft profiles are shown in Figure 1. The imposed zonal wind profile indicates a strong low level jet which implies strong shear in the lowest 2–3 km near the surface. The imposed vertical

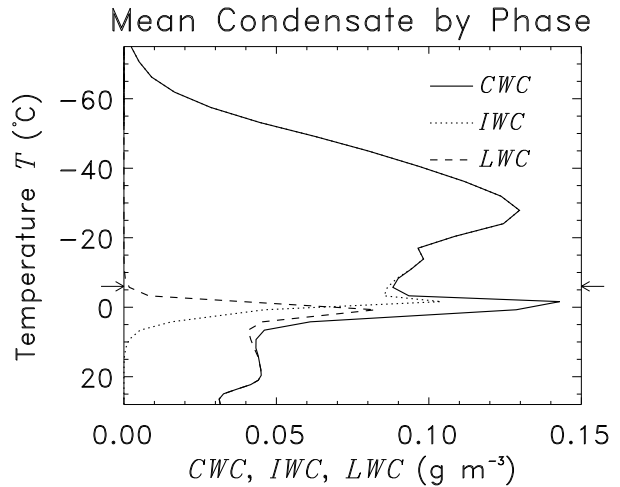


Figure 3. Time- and domain-average ice (dotted), liquid (dashed), and total (solid) condensate (g m^{-2}) from the 24 day CEM simulation. Horizontal arrows indicate the 500 mb level.

velocity profile peaks in the mid to upper troposphere at 3 cm s^{-1} upward motion.

The CEM simulation was run for 24 days. The length of integration was chosen to insure that the model reached an equilibrium with the large scale forcing. The time evolution of domain-average temperature and precipitable water showed the model takes roughly 15 days to reach equilibrium with the large scale forcing [Figure 4, Grabowski et al., 1995]. Figure 2 shows the snapshot of total condensate mixing ratio q_c at the end of day one. The figure indicates two convective cores located near 50 km and 350 km with extensive upper tropospheric cloud cover. The time-averaged (days 4–24) and domain-averaged concentrations for liquid water, ice water, and total condensed water are shown in Figure 3. Above 500 mb, the cloud water is dominated by ice, with ice concentrations between 0.1 and 0.14 g m^{-3} . Note that the model predicts a very sharp transition between liquid and ice phase. In terms of temperature this transition occurs over only 5 °K.

As discussed in the next section, we have employed the results from this CEM simulation to develop a prognostic scheme for anvil cloud. The advantage of using this model is it provides a self-consistent and comprehensive data base for testing and developing parameterizations for the GCM. However, we recognize the CEM model should itself be validated with

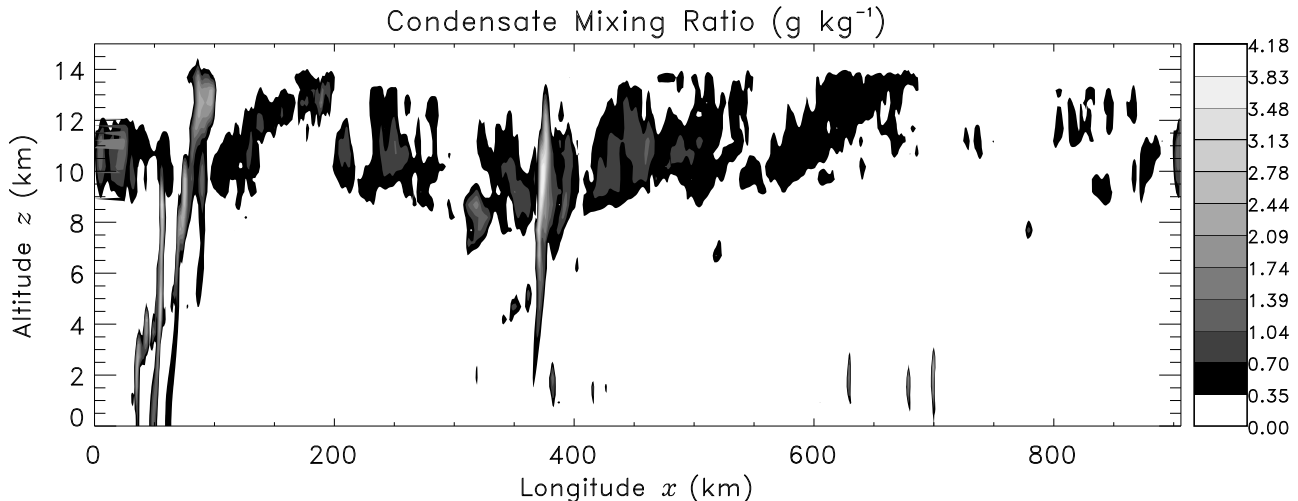


Figure 2. Snapshot of condensed water mixing ratio q_c (g kg^{-1}) at the end of day 1 of the CEM simulation.

observational data. We hope these data will become available in the not too distant future.

3. Parameterization of Ice Condensate Resulting from Convection

3.1. Source Processes Deduced from the CEM Dataset

A number of dynamic and thermodynamic fields were considered as proxies for the generation of anvil ice water. Time series of the mean convective (cumulus) mass flux, relative humidity, cloud amount (fraction), and ice water content were compared to the time tendency of total column ice water path, IWP. Xu and Krueger [1991] concluded convective mass flux M best predicts tropical convective cloud amount and the IWC of individual anvil layers. Our analyses indicate M also best predicts IWP. This conclusion is widely applicable to GCMs because many, if not most, cumulus convection parameterizations predict M [e.g., Arakawa and Schubert, 1974; Tiedtke, 1993; Zhang and McFarlane, 1995]. We restrict the present study to the actual parameterization of IWP in terms of M . In the context of the CEM, M is defined to be the horizontally averaged vertical density flux from all grid cells which exceed a critical updraft ($w > w_c = 1 \text{ m s}^{-1}$) and a critical condensate amount ($q_c > q_{c,c} = .05 \text{ g kg}^{-1}$). The optimal choice of w_c and $q_{c,c}$ depends on the GCM convective parameterization, see Section 4 below.

Figure 4 shows the simultaneous variation of M at 500 mb and IWP through the first day of the simulation. The initial anvil formation, lasting about six hours, occurred as a prescribed thermal instability triggered concentrated convective updrafts (cores) which detrained frozen condensate into a cirrus anvil above 500 mb. The variation of IWP is strongest during convectively active periods, and subdued during the convectively quiescent period ($400 < t < 900 \text{ min}$). Non-convective formation of anvil ice is also evident during the quiescent period. Secondary circulations and weaker convection ($w < 1 \text{ m s}^{-1}$) apparently result in significant deposition. These mesoscale processes are poorly understood, but consistent with budget studies [Leary and Houze, 1980]. At $t \approx 900 \text{ min}$ two widely separated, westward travelling convective systems developed and maintained distinct anvils. Deep convective activity similar to $900 < t < 1300 \text{ min}$ occurred approximately daily and maintained extensive anvil coverage for the remaining three weeks.

In order to isolate the processes controlling ice generation from destruction we focused on the initial hours of anvil formation, when a single convective tower dominated the mass budget of the entire domain. Figures 4b and 4c show initial anvil formation is attributable to the strength of M near the freezing level. We define p_c as the pressure p at which M most strongly correlates with IWP. Similar analyses (not shown) which varied p from 750 to 250 mb, confirmed $p_c \approx 500 \text{ mb}$ (roughly 50 mb above the trop-

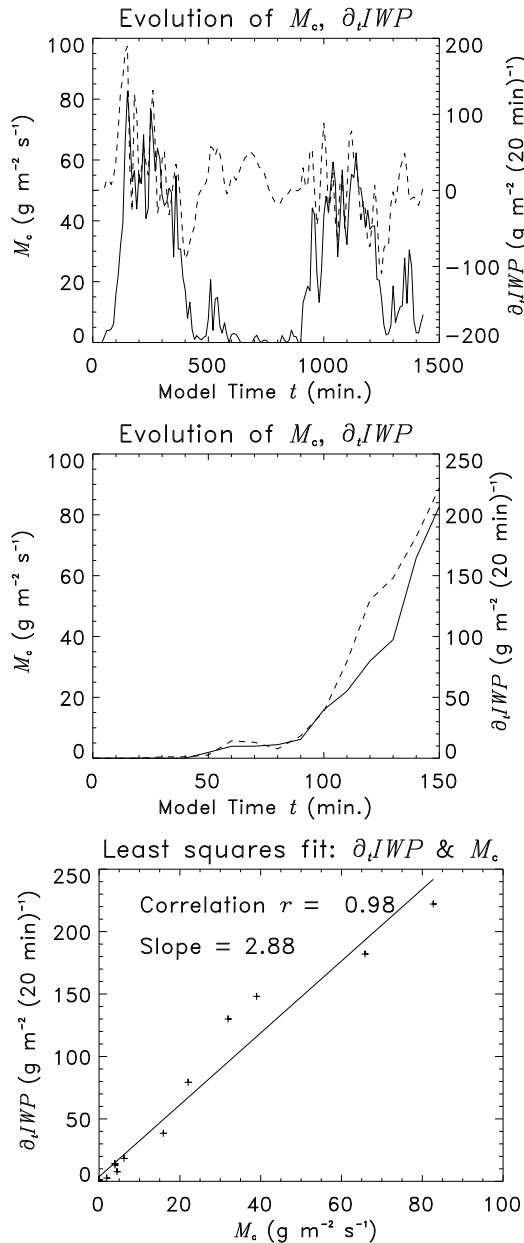


Figure 4. (a) Evolution of 500 mb M (g m^{-2}) (solid) and IWP (dashed) during the first 24 hours of the CEM simulation. IWP is expressed in $\text{g m}^{-2} (20 \text{ min})^{-1}$, i.e., mass change per GCM timestep. (b) The first 2.5 hours of (a). (c) Linear correlation and least squares fit of 500 mb M to IWP from (b).

ical freezing level). Deep convection was perennial in the three week simulation but $M_c \equiv M(p_c)$ never exceeded $80 \text{ g m}^{-2} \text{ s}^{-1}$. This adds confidence the correlation between M_c and IWP in Figure 4c is robust over the realizable range of convective intensities. On this basis we adopted M_c as the fundamental predictor of anvil ice generation by convective processes. This is implemented in ANV as the term $c_1 M_c$ in forecast equation (1) for q_i (shown below). Ice generated by convection may be augmented by stratiform condensate (detailed in Section 5) in non-convecting layers.

The current ANV implementation apportions new IWP ($c_1 M_c \Delta t$) evenly among all convecting layers where $T < 0^\circ \text{C}$. Experimental versions of ANV, employing the convection scheme of Hack [1994], apportioned new IWP weighted by local M , so that IWP was distributed nonuniformly. This method tended to overpredict q_i at near freezing level at the expense of too little q_i in the upper levels of anvils. Other methods of distributing IWP nonuniformly in the vertical are expected to become more practical as data from field observations, especially in the tropics, accumulates. For example, new IWP could be vertically partitioned based on observed IWC profiles.

3.2. Sink Processes Deduced from the CEM Dataset and Observations

A forecast equation for q_i requires adequate representation of ice removal processes to balance the convective detrainment. We divide sink processes into three terms: precipitation, sublimation, and sublimation of precipitation. Isolating the specific processes causing anvil decay in the CEM simulation was difficult due to persistent convection and secondary circulations in the domain (Figure 4a). Nevertheless, regressions of relative humidity, saturation deficit, cloud amount, and IWC against IWP and IWC were performed to identify the most promising proxies for anvil decay.

Precipitation (including virga and mesoscale downdrafts) is the strongest sink process in anvils [Leary and Houze, 1980; Gallus and Johnson, 1991]. Cloud amount at 500 mb (determined using the method of Sui et al. [1994]) was clearly related to IWP throughout the convectively quiescent period. Despite this, cloud amount was discarded as a proxy for precipitation because it is difficult to define consistently from CEM to GCM. There are three advantages meriting IWC as the chief predictor for the rate of precipitation: First, Heymsfield [1977] found the precipita-

tion rate in deep continental ice cloud was proportional to $IWC^{1.16}$. Second, IWC often nicely (anti-)correlated with IWC in the CEM (correlation was often enhanced by letting IWC lag IWC by 40–60 min). However, no useful rate coefficient could be isolated because the archived data lacked necessary fields. Third, IWC and precipitation rate are independent of the horizontal extent of a homogeneous anvil; thus a rate coefficient derived from a SRCM applies to a GCM. On this basis ANV converts ice to precipitation (snow) at a rate proportional to anvil mass, $c_3 q_i$. The value of the free parameter c_3^{-1} , the e-folding time for ice removal due to precipitation, is discussed in Section 5 below. Currently, precipitation in ANV instantly falls through the column. Smith [1990] describes a simple method for implementing realistic fall-speeds, which can significantly change the amount of ice in a GCM [Senior and Mitchell, 1993]. A Kessler-style formulation sublimates precipitation (virga) [e.g., Sundqvist, 1988].

Anvil decay through local sublimation includes the effects of entrainment of dry air into cloudy, and sub-grid scale distributions of cloudiness and subsaturated air. Neither the ice saturation deficit ($q_{vi} - q_v$) nor the relative humidity (RH) correlated with IWC after the upper troposphere equilibrated to $RH \sim 100\%$ [Grabowski et al., 1995]. Rather than resorting to a sub-grid scale model of q_{vi} distribution (i.e., cloud fraction), we take a semi-empirical approach like Donner [1993]. Following Leary and Houze [1980], many studies have inverted observations of tropical and continental convective systems to infer the spatially and temporally averaged moisture balance between the convective and stratiform regions. Gallus and Johnson [1991], in their Table 2, summarize the ratio between mesoscale (anvil) evaporation (E_{me}) and precipitation (R_m) from five such studies. The average E_{me}/R_m in tropical and continental systems is .22 and .28, respectively. On this basis ANV assumes that the ratio of anvil sublimation to precipitation is $c_2/c_3 = .25$ in every layer and timestep.

3.3. Prognostic Thermodynamic Equations of ANV

Figure 5 shows a conceptual model of the ice budget in ANV. For a grid cell of density ρ , thickness Δz , ice mixing ratio q_i , vapor mixing ratio q_v , temperature T , ice saturation mixing ratio q_{vi} , precipitation (snow) flux P_1 , and large scale wind field \vec{u} , the ther-

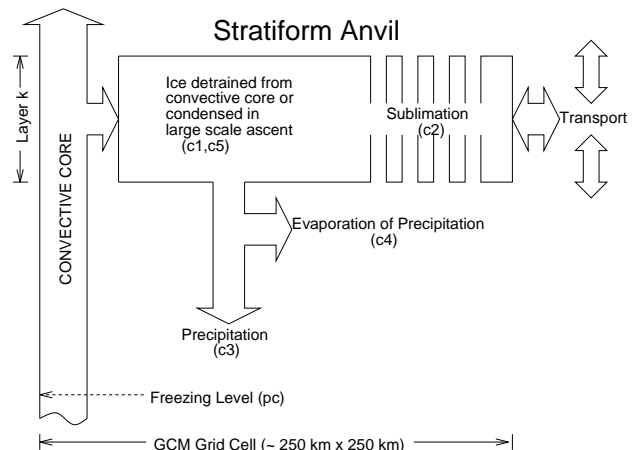


Figure 5. Conceptual model of the ice budget in ANV. Free parameters c_1 – c_5 and p_c are defined and discussed in Sections 3–5 and used in equations (1–6).

modynamic couplings that define ANV are:

$$\frac{Dq_i}{Dt} = \frac{c_1 M_c}{\rho \Delta Z} - c_2 q_i - c_3 q_i \quad (1)$$

$$\frac{Dq_v}{Dt} = -\frac{c_1 M_c}{\rho \Delta Z} + c_2 q_i + c_4 \left(1 - \frac{q_i}{q_{vi}}\right) P_1^{1/2} \quad (2)$$

$$\frac{DT}{Dt} = \frac{L_{vi}}{c_p} \left[\frac{c_1 M_c}{\rho \Delta Z} - c_2 q_i - c_4 \left(1 - \frac{q_i}{q_{vi}}\right) P_1^{1/2} \right] \quad (3)$$

where ΔZ is the thickness of the convecting portion of the column in which $T < 0^\circ\text{C}$, L_{vi} is the latent heat of sublimation, and c_p is the specific heat of air at constant pressure. The material derivatives on the LHS of (1–3) account for advection by \vec{u} . The first term on the RHS of (1) relates the generation of total column ice to M_c . The second term represents local sublimation of the anvil due to sub-grid scale entrainment and subsaturation. The c_3 term in (1) converts ice to precipitation. The c_4 term in (2) and (3) acts to sublime precipitation. Terms not involving ice have been omitted from the RHS of (2) and (3). Note that the detraining anvil completely covers a gridcell, i.e., cloud fraction is 1. Table 1 summarizes all the parameters used by ANV.

4. Meshing ANV with a GCM

Meshing an anvil parameterization from a CEM into a GCM only makes sense if an equivalence can be demonstrated between the predictive parameters in the respective models. Since M_c is the sole source

	Meaning	Suggested Value	Source
c_1	Relates M_c to mesoscale detrainment	2.4×10^{-3}	CEM, Figure 4c
c_2	Anvil sublimation rate	$.25c_3 \text{ s}^{-1}$	Empirical ^a
c_3	Precipitation rate	$2.8 \times 10^{-4} \text{ s}^{-1}$	SRCM, Figure 9
c_4	Precipitation sublimation rate	$1 \times 10^{-5} \text{ m kg}^{-1/2} \text{ s}^{-1/2}$	Empirical ^b
c_5	Relates stratiform \dot{q}_i to w , T	-1.15	SRCM, Figures 10,11
w_c	Threshold w for convection in CEM	1 m s^{-1}	CEM, GCM, Figure 8
$q_{c,c}$	Threshold q_c for convection in CEM	$.05 \text{ g kg}^{-1}$	CEM, Empirical
p_c	Level to evaluate M for (1-3)	500 mb	CEM, Figure 4b

Table 1. Free parameters in ANV

of convectively generated ice in ANV (1), the CEM M profile should match the GCM M profile to ensure ANV complements, not co-opts, the GCM convection scheme. The M predicted by a GCM moist convection scheme sums the mass flux from all sub-grid-scale (non-resolved) convective elements (clouds). Convection in the GCM context includes all unresolved mass flux generated by moist adiabatic instabilities. However, the continuous physical processes in a CEM do not distinguish between convection, mesoscale eddies, and large scale ascent. As mentioned above, ANV employs a threshold updraft w_c and threshold condensate mixing ratio $q_{c,c}$ to select GCM-type convection in the CEM; only gridcells exceeding these thresholds contribute to CEM M . The main criterion for setting these thresholds is to obtain consistent M between models (and, hopefully, observations) so that implementations of (1-3) in the GCM will behave predictably.

Intercomparing the convective behavior of a CEM to a GCM raises a number of questions. How can the influence of differing boundary conditions between the CEM (periodic, fixed SST) and a GCM region (open, prescribed SST) be minimized? How might the internal variance of the models (their sensitivity to initial conditions) skew the analyses? The models run at physically incommensurate temporal and spatial scales; is it feasible to use the instantaneous GCM M_c in (1-3)? We attempt to address these issues in three ways. First, we isolate a common synoptic regime to intercompare. Second, we look for systematic convection differences in averages over many convective system lifetimes. Third, we intercompare frequency distributions of the instantaneous M_c used in (1-3).

4.1. GCM Control Simulation

We employ a new version of the NCAR CCM2 (hereafter the GCM) to demonstrate the technique of mapping (1-3) to a GCM in a physically consistent manner. The GCM contains four improvements over the standard CCM2 [Hack et al., 1993] in the area of cloud physics: Ice phase condensate is treated with the radiative scheme of [Ebert and Curry, 1992]. A continental/maritime distinction is made in the effective radius of cloud droplets [Kiehl, 1994b]. LWP is based on column precipitable water rather than prescribed by latitude. Large scale precipitation is able to evaporate between the cloud and surface.

Steady conditions from the Marshall Islands region studied by Yanai et al. [1973] were used to force the CEM simulation (Figure 1). July GCM simulations best matched the strong low-level convergence and intense precipitation of the CEM simulation in a $10^\circ \times 15^\circ$ region centered at 125°E , 15°N (in the Philippine Sea, 40°W of the Marshalls). This control region consists of 19 maritime and one land gridpoint at T42 resolution ($\sim 2.8^\circ$). The GCM simulation was run for 14 days and instantaneous data were archived every timestep ($\Delta t = 20 \text{ min}$). Land-locked precipitation (10% of the regional total) was removed by excising the land gridpoint (the CEM simulation was also entirely maritime). Figure 6 compares the resulting instantaneous, domain-averaged precipitation timeseries between CEM and GCM. The mean precipitation rates (and associated latent heating) are similar: 14.4 and 17.0 mm d^{-1} , respectively. However, the strong diurnal component in the CEM contrasts markedly with the low-frequency synoptic events in the GCM. The significant difference in the spectral

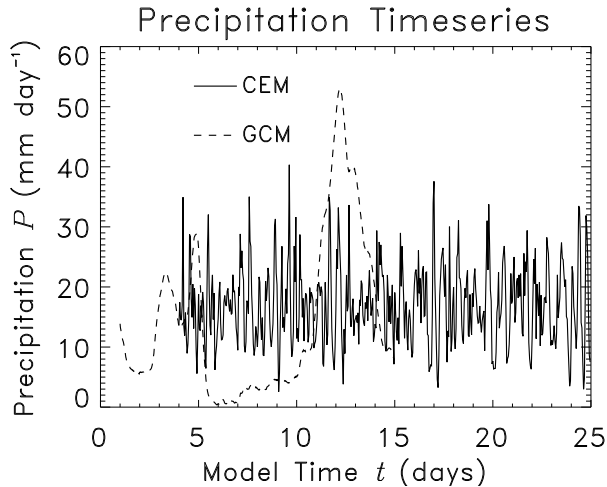


Figure 6. Domain-averaged precipitation timeseries (mm d^{-1}) from tropical simulations. CEM instantaneous hourly values from days 4–24 (solid) and GCM instantaneous values every 20 m for 14 days (dashed). Offset along the abscissa is arbitrary.

characteristics of the latent heating raised doubts that the M profiles would be comparable.

4.2. Threshold Convective Velocity

Intercomparing temporally and spatially averaged M profiles reduces, to the extent possible, model differences due to internal variability. Figure 7 compares the vertical structure of M in the GCM control region, the CEM simulation, and the Marshall Islands as inferred by Yanai et al. [1973]. Observed M peaked at the surface with a secondary maxima near 250 mb, indicative of anvil circulations. Strong low level convergence and shear cause M to peak near the surface in the Yanai and GCM M profiles. In contrast, the closed domain forces CEM M to zero at the surface (cf. Figure 18 of Sui et al. [1994]). The GCM and CEM reproduce observed M from the boundary layer to 500 and 600 mb, respectively. The weak GCM M in the upper troposphere is a known bias of the convection scheme, see Mahowald et al. [1995]. CEM M is sensitive to w_c and $q_{c,c}$ (all figures in this study use $w_c = 1 \text{ m s}^{-1}$ and $q_{c,c} = .05 \text{ g kg}^{-1}$). Decreasing $q_{c,c}$ from .1 to 0 g kg^{-1} nearly doubled M beneath 500 mb. Above 500 mb however, M is relatively insensitive to $q_{c,c} < .1 \text{ g kg}^{-1}$ because the CEM simulation produced persistent anvil coverage in this region (Figure 3). The modeled 800–200 mb M gradient is

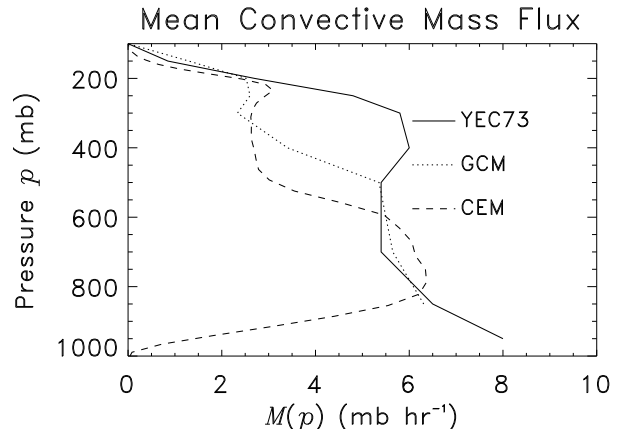


Figure 7. Time- and domain-average convective mass flux M (mb hr^{-1}) over the Marshall Islands region from observations (solid), GCM (dotted), and CEM (dashed). Updrafts are defined to be positive. Observations are taken from Yanai et al. [1973], Figure 13.

too strong. Halving w_c from 1 to $.5 \text{ m s}^{-1}$ reduced the CEM gradient from 2.5:1 to 1.25:1, in agreement with Yanai. The relaxed gradient was caused by including a strong, perhaps radiatively driven, circulation ($.5 < w < 1 \text{ m s}^{-1}$) near anvil top.

The radiative and dynamical feedbacks from prognosed cloud are nonlinear. Therefore it is important that the temporal distribution of GCM M match the distribution of CEM M used to derive (1–3) and to pick c_1 . Figure 8 shows histograms of the instantaneous, domain-average M from the CEM and GCM. The frequency distributions of M in the two models were most similar from 500–200 mb using $w_c = 1 \text{ m s}^{-1}$. Relaxing w_c increases the mean and mode of M_c . Typically only 1–2 % of the (2-dimensional) CEM domain satisfied $w > 1 \text{ m s}^{-1}$. This fraction is at the low end of satellite-derived estimates of the areal extent of deep convective cloudiness [Fu et al., 1990].

The overall agreement in the simulated M profiles is somewhat unexpected, considering the differences between the models and their precipitation timeseries (Figure 6). The agreement in mean M (Figure 7) partially results from tuning $q_{c,c}$ and w_c , but the underlying distributions of M (Figure 8) were already similar. Both $q_{c,c}$ and w_c depend on the GCM convection scheme with which ANV is to be used, and possibly on the synoptic regime.

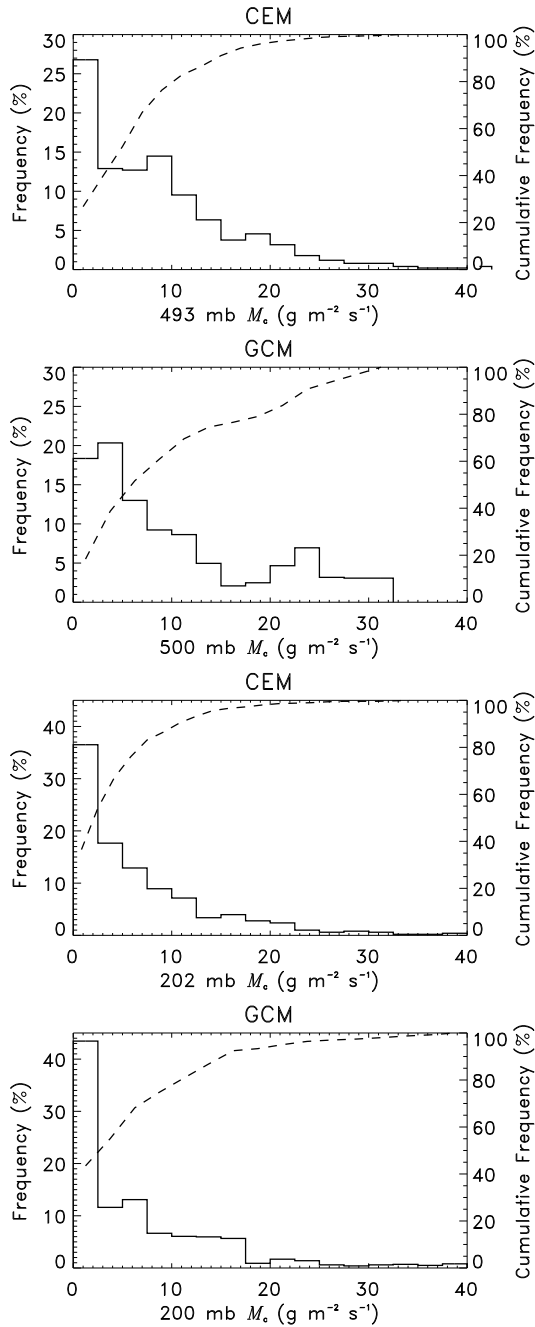


Figure 8. Comparison of frequency distribution of instantaneous M ($\text{g m}^{-2} \text{s}^{-1}$) between CEM and GCM. The left hand axes indicate the percentage of the data contained in each bin. The dashed lines and right hand axes indicate the percentage of the data with M less than the abscissa. (a) CEM \sim 500 mb. (b) GCM 500 mb. (c) CEM \sim 200 mb. (d) GCM 200 mb.

5. Stratiform Ice Cloud Generation

Orographically forced uplift, warm frontal overrunning, and large scale ascent and cooling can form ice cloud in the absence of any parameterized convection; we denote such ice as stratiform. The GCM-resolved thermodynamic fields that control the development of stratiform (stable) ice cloud are temperature T , humidity q_v , and updraft w [Heymsfield and Donner, 1990]. As with convective condensation, the temporal and spatial scales of stratiform condensation differ vastly from the scales on which GCMs predict the thermodynamic fields. GCM schemes for diagnosis and prognosis of stratiform ice span a corresponding range of complexity: Heymsfield and Platt [1984] empirically relate q_i to w and T . Sundqvist [1988] predicts q_i from highly parameterized physical processes which assume exact saturation in the cloudy fraction of a gridbox. Heymsfield and Donner [1990] diagnose q_i by trajectory integrations of the thermodynamics governing single parcel behavior. Smith [1990] predicts q_c by assuming a functional form for the sub-gridscale distribution conserved quantities. Feingold and Heymsfield [1992] diagnose q_i from fits to a detailed microphysical scheme to determine number concentration, effective radius, and q_c for liquid (or spherical ice crystal) cloud. Experience with the above methods suggests detailed sub-gridscale modelling may not be necessary to predict free-atmosphere stratiform condensation at GCM resolution. Our strategy for modelling stratiform condensation is to replace the mass flux-based creation process from (1) with a quiescent deposition process, but to keep the same destruction and removal processes.

5.1. Closure and Microphysical Assumptions

Parameterization of stratiform condensation in large scale models involves closure assumptions and microphysical assumptions. Allowing cloud formation in subsaturated gridcells requires a closure assumption to relate the resolved thermodynamic fields to the sub-gridscale distribution of condensate. Stratiform cloud fraction A_s is naturally suited to map column (and parcel) models of stratiform condensation, which is horizontally homogeneous, to specified horizontal fractions of a gridcell. Numerical studies by Xu and Krueger [1991] suggest relative humidity is best suited to diagnose A_s . At the same time, diagnoses of A_s based on local or synoptic atmospheric state continually improve as field, model, and satellite

data accumulate. To accommodate future advances in A_s diagnosis, and to maintain internal simplicity, ANV requires the GCM to make the closure assumptions for, and to specify, A_s . The rest of this section describes the microphysical assumptions we make to model condensate formation and removal processes.

A supersaturated vapor field quickly equilibrates by deposition, assuming adequate ice freezing nuclei (IFN) are present. The IFN assumption is justified in most cases for $T < -15$ °C [Heymsfield and Donner, 1990]. Since supercooled droplets should be represented by the liquid component in a full GCM cloud scheme, ANV assumes all vapor condensed at $T < 0$ °C to form ice. Complications arise from droplet curvature (Kelvin) effects, water inhomogeneity (solute) effects and radiation (especially at cloud base and top). These processes slightly change the equilibrium vapor pressure over crystals and lead to size-based competition for vapor among ice crystals [Ramaswamy and Detwiler, 1986]. Bulk (non size-resolving) condensate models such as ANV may ignore vapor competition so long as the timescale for the vapor field to equilibrate with ice crystals through diffusional processes is much faster than a typical GCM timestep ($\Delta t \sim 20$ min).

The balance between q_i and q_v in a fixed, horizontally homogeneous, exactly saturated layer in an updraft w is:

$$\frac{\partial q_i}{\partial t} = -\frac{\partial q_{vi}}{\partial t} - w \frac{\partial q_{vi}}{\partial z} - w \frac{\partial q_i}{\partial z} - c_2 q_i - c_3 q_i \quad (4)$$

The first two terms on the RHS of (4) describe the changes in vapor available for deposition in large-scale ascent due to local temperature change (e.g., adiabatic or radiative cooling of the layer), and convergence of supersaturated vapor, respectively. The difficulty of separating the contributions of w and T to deposition in an Eulerian framework is apparent in these two terms: vapor flux and adiabatic cooling are linear in w , but q_{vi} is exponential in T due to the Clausius-Clapeyron relationship. The next term is the large scale convergence of q_i . The remaining terms are local sublimation and precipitation, parameterized in terms of q_i from (1). The behavior of \dot{q}_i in the limit of resolved and saturated large-scale ascent (4) guides our parameterization of sub-gridscale effects.

5.2. Size Resolving Column Model (SRCM) Simulations

Sensitivity studies were performed with the SRCM of Zender and Kiehl [1994] in order to isolate the effects of updraft speed w from temperature T in (4). The SRCM explicitly represents nucleation, deposition, sublimation, sedimentation, and radiation, but does not attempt represent diffusion, convection, collision, liquid processes, or entrainment. The SRCM used 50 geometrically spaced mass bins for ice particles corresponding to hexagonal column lengths 3–2000 μm . The time step is 3 s for microphysics and transport, 1 min for radiation. The thermodynamic profile was a standard 35-level tropical atmospheric profile from ICRCM [Ellingson et al., 1991] with an embedded 130-level ($\Delta z = 100$ m) computational grid from 5–18 km. The ice crystal distribution from a decaying tropical anvil [Knollenberg et al., 1993] was replicated to form a 2 km thick (\sim one GCM layer) homogeneous anvil with initial IWP ≈ 73 g m^{-2} . Most uncertain in the Knollenberg distribution is the abundance of small ice crystals (which contribute little to cloud mass). The following sensitivity studies are presented in terms of IWP rather than q_i ($= \text{IWP}/(\rho \Delta z)$) for direct comparison to Figure 4, and to simplify deductions about the radiative import of the sensitivities.

5.3. Timescale for Precipitation

As mentioned in Section 3, the precipitation rate of cirrus is taken to be proportional to cloud mass itself. The proportionality constant, c_3 in (1), is the inverse of the e -folding timescale τ for sedimentation of ice crystals in the cloud. Modelling the sedimentation of a tropical anvil in the SRCM provides an understanding of the range of τ in the atmosphere. Here we use the term *sedimentation* rather than *precipitation* to emphasize the SRCM does not account for collection processes. This study monitored the IWP change in the initial cloud through a six hour integration in still, saturated air. Figure 9 shows the sedimentation of the same anvil from three different cloud base heights. The two solid curves represent purely exponential decay of the initial anvil, $\text{IWP}(t) = \text{IWP}_0 e^{-t/\tau}$, with timescales $\tau = .5$ and 2 hr. The SRCM employs terminal velocities from Heymsfield [1972], which increase with height and crystal length. Sedimentation is very efficient for the first hour, as the large crystals ($L > 200$ μm) quickly fall from the anvil. Differential sedimentation causes the separation of the dashed curves before $t = 2$ hr, and leaves more vapor

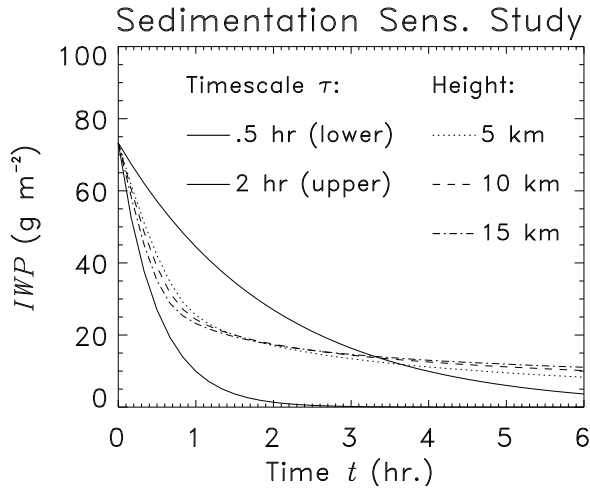


Figure 9. Time variation of IWP (g m^{-2}) for the same initial 2 km thick anvil at three different cloud base heights: 5 km (dotted), 10 km (dashed), and 15 km (dot-dashed). Solid curves represent pure exponential decay with timescale $\tau = .5$ hr (lower) and 2 hr (upper), respectively.

available for deposition to small crystals afterwards. The remaining mass descends slowly ($< 30 \text{ cm s}^{-1}$) in smaller crystals. Figure 9 shows that Near GCM resolution in the free troposphere ($\Delta z < 2 \text{ km}$), figure 9 shows $\tau < .5$ hr overestimates sedimentation for the entire life of the anvil while $\tau > 2$ hr underestimates sedimentation of large crystals, and hence cloud mass. A compromise value of $\tau = c_3^{-1} = 1$ hr is recommended. This should be contrasted with observed “typical” anvil lifetimes of ~ 6 hr over Panama [Ackerman et al., 1988]. Of course observations implicitly include condensate resupply through convective detrainment, mesoscale generation, and cloud top cooling.

5.4. Dependence of Deposition Rate on Updraft

This sensitivity study isolates the effect of updraft on stratiform condensation by examining the growth of the initial cloud in an atmosphere exactly saturated with respect to ice. Ice crystals were not allowed to sediment. Figure 10a shows the dependence of IWP on the ascent speed w of vapor for the same initial anvil at three different cloud base heights. IWP is computed from the difference between the final and initial (73 g m^{-2}) IWP from one hour integrations of

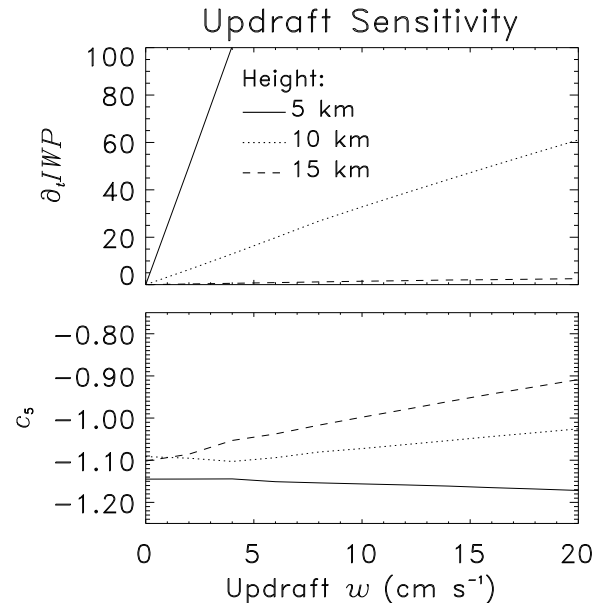


Figure 10. Sensitivity of (a) deposition rate \dot{IWP} and (b) c_5 to updraft w (cm s^{-1}) in a 2 km thick anvil in a saturated column. IWP is expressed in $\text{g m}^{-2} (20 \text{ min})^{-1}$, i.e., mass change per GCM timestep. Results are shown for three different cloud base heights: 5 km (solid), 10 km (dotted), and 15 km (dashed).

the SRCM. IWP is linear with w for all cloud heights, and a nonlinear dependence on cloud height is evident. Most of the difference ($> 90\%$) in ice deposition rates stems from the exponential decrease in $-\partial q_{vi}/\partial z$ in (4) from 1.4 to .02 g kg⁻¹ km⁻¹ between 5 and 15 km. The ambient density decrease from .63 to .24 kg m⁻³ between 5 and 15 km accounts for the remaining factor of ~ 3 difference in the deposition rates. The IWP shown is an upper bound because the initial atmosphere was saturated and all removal processes were disabled.

Evidently a simple linear dependence of IWP on w will not capture the effects of T . Instead, we define a single parameter approximation that includes both T and w effects. We implicitly define the dimensionless empirical parameter c_5 based on the second term on the RHS of (4):

$$\frac{\partial q_i}{\partial t} \equiv c_5 w \frac{\partial q_{vi}}{\partial z} \quad (5)$$

Thus c_5 expresses the ice formation tendency as a function of supersaturated vapor convergence alone. Note that $\partial q_{vi}/\partial z$ is analytically tractable; it depends only on T [e.g., Washington and Parkinson, 1986]. Figure 10b shows c_5 computed using the initial, not the instantaneous, T profile. This removes the feedback of heating of the cloud environment on $\partial q_{vi}/\partial z$ (but not on $\partial q_i/\partial t$). Clearly c_5 is relatively constant because the linear w and exponential T dependencies are factored out.

5.5. Dependence of Deposition Rate on Temperature

This sensitivity study isolates the effect of cloud temperature on stratiform deposition. As in the updraft sensitivity study, the atmosphere is exactly saturated with respect to ice and sedimentation of ice crystals was disabled. Figure 11a shows the dependence of IWP on the mid-cloud temperature T . As expected from (4), the deposition tendency is exponential in T , while the spacing between the curves is linear in w . Exponential dependence of IWC on T characterizes observations of cirrus formed by large scale ascent [Heymsfield, 1977].

Figure 11b shows the empirical parameter c_5 from (5) falls in nearly the same range as the updraft sensitivity study (cf. Figure 10b). Indeed, c_5 varies $\lesssim 20\%$ for typical upper tropospheric ice cloud. The spread in c_5 is dominated by variations in the lapse rate in the ICRCCM T profile, which changes local advective cooling, and by the associated saturation

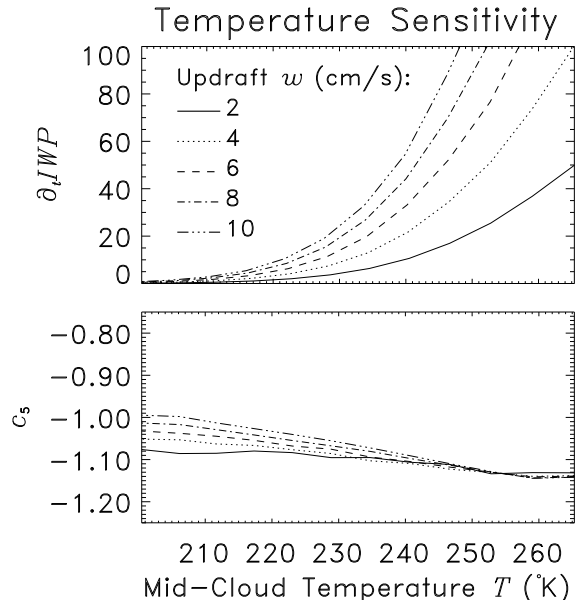


Figure 11. Sensitivity of (a) deposition rate IWP and (b) c_5 to mid-cloud temperature T in a 2 km thick anvil in a saturated column. IWP computed and scaled as in Figure 10. Results are shown for vertical motions of 2, 4, 6, 8, and 10 cm s⁻¹.

vapor density, which determines the mass available for deposition. When c_5 is computed using instantaneous T (not shown), the advectively cooling environment reduces $|\partial q_{vi}/\partial z|$ and increases $|c_5|$ by $\sim 20\%$ to $-1.1 < c_5 < -1.2$. This effect is more pronounced at higher altitudes where tropical lapse rate and vapor density are smaller, but can be ameliorated by horizontal circulation and diabatic heating.

In summary, the slight variation of c_5 over a wide range of w and T is appealing for parameterization purposes. Therefore ANV models gridbox stratiform deposition due to large scale ascent as $A_s c_5 w \partial q_{vi}/\partial z$. We recommend $c_5 = -1.1$ for representing light ($w < 10$ cm s⁻¹) ascent between 5–10 km in altitude, where a GCM stratiform ice scheme is most active.

The full equation for stratiform ice in ANV is

$$\frac{Dq_i}{Dt} = A_s c_5 w \frac{\partial q_{vi}}{\partial z} - c_2 q_i - c_3 q_i \quad (6)$$

where A_s is the GCM-supplied stratiform cloud fraction. In non-convecting gridcells with $w > 0$, (6) is used in place of (1), along with (2) and (3). A_s fills the role of $\partial q_{vi}/\partial t$ in (4), to some extent, because local changes in temperature will presumably affect A_s and

thus \dot{q}_i through (6). Note (6) does not produce ice in still air ($w = 0$). In practice stable cloud fraction A_s produced by many GCM cloud schemes is also zero in still or subsiding air. Set $A_s = 1$ in subsiding air to allow sublimation. Stratiform cloud in moist, radiative cooled regions above anvils may be underpredicted by ANV because (6) lacks stability dependence and $w \rightarrow 0$ near the tropopause. As mentioned in Section 3, the sublimation rate $c_2 q_i$ is determined (as a fraction of the precipitation rate $c_3 q_i$) from budget studies which implicitly contain the effects of partial cloudiness. Thus the precipitation and sublimation rates in (6) act independently of cloud fraction A_s , exactly as in (1).

The stratiform cloud ANV attempts to represent in a GCM gridbox can be envisioned as maintained by some unknown, underlying distribution of sub-grid-scale updrafts (and downdrafts) with mean speed w . The range of w in Figure 10, 0–20 cm s⁻¹, is approximately that reported by Heymsfield and Platt [1984]. Large scale ascent in nonconvecting gridcells at the GCM scale is typically < 5 cm s⁻¹. The sub-grid-scale distribution composing w could, if known (e.g., a Poisson distribution with a certain variance), be convolved through the c_5 term in (5) to obtain a more realistic \dot{q}_i . Lacking this information, we assume the effects of sub-grid-scale distributions of w on \dot{q}_i are incorporated through A_s .

6. Discussion

We have presented the rationale for, and development of, an ice cloud parameterization suitable for a GCM representation of ice cloud based on modeled and observed behavior of tropical anvils. The methodology of the development is explicit parameterization of the physical processes of ice cloud formation and removal: detrainment of convectively formed ice into a stratiform anvil, formation of ice through large scale ascent, sublimation, precipitation, and evaporation of precipitation. Each process was simply modeled in terms of a prognostic GCM variable and a single free parameter and incorporated into GCM forecast equations for cloud ice, water vapor, and temperature. Each free parameter was determined by a sensitivity study that attempted to isolate the respective process. The exception is the parameter determining local sublimation (c_2); it was chosen to match empirical estimates of anvil contributions to tropical convective system hydrologic budgets.

ANV is intended to be the ice phase component

of a GCM cloud scheme. It can be wedded to the liquid component of a full cloud scheme by use of a parameterization for the fraction of condensate that is ice. Many of the physical processes and assumptions underpinning ANV would need only with minor modifications to be suitable for a prognostic liquid water scheme. Although we have not done so here, one could perform analogous single parameter sensitivity studies for \dot{q}_i in terms of M_c , w and T .

We have taken advantage of a hierarchy of models (SRCM, CEM, and GCM) and the empirical budget estimates because no single tool was wholly adequate. This methodology demonstrated the feasibility of combining the results from a hierarchy of models and observations into a coherent cloud parameterization. We eschewed incorporating detailed sub-grid-scale models into ANV although we recognize such models (e.g., cloud fraction) enhance the internal consistency of a condensate forecast. The emphasis has been on forecasting ice sequestered in mesoscale anvils associated with deep convection because anvils' combination of areal extent, longevity, and IWP produces strong radiative forcing. However, budget studies infer 25–60% of anvil ice comes from mesoscale updrafts outside the convective core region [Leary and Houze, 1980; Gallus and Johnson, 1991]. This ice is only implicitly parameterized by the c_1 term in (1) and the c_5 term in (6). Future studies should attempt to explicitly parameterize the ice formation by intra-anvil circulations, perhaps in terms of radiative heating gradients, stability, q_i , and w .

Acknowledgments The authors wish to thank G. Tripoli for supplying the CEM, and J. Doetzel for programming support. CSZ gratefully acknowledges discussions with W. Grabowski and J. Petch, and guidance in cloud parameterization from P. Rasch. This work was supported in part by DOE Atmospheric Radiation Measurements Program grant DE-AI05-92ER61376 and by NASA Earth Observing System project W-17,661.

References

- Ackerman, T. P., K.-N. Liou, F. P. J. Valero and L. Pfister, 1988: Heating rates in tropical anvils. *J. Atmos. Sci.*, **45**(10), 1606–1623.
- Arakawa, A. and W. H. Schubert, 1974: Interaction of a cumulus cloud ensemble with the large-scale environment: Part I. *J. Atmos. Sci.*, **31**, 674–701.

- Browning, K. A., 1994: Survey of perceived priority issues in the parametrizations of cloud-related processes in gcms. *Q. J. R. Meteorol. Soc.*, **120**, 483–487.
- Del Genio, A. D., M.-S. Yao, W. Kovari and K. K.-W. Lo, 1996: A prognostic cloud water parameterization for global climate models. *J. Clim.*, **9**(2), 270–304.
- Donner, L. J., 1993: A cumulus parameterization including mass fluxes, vertical momentum dynamics, and mesoscale effects. *J. Atmos. Sci.*, **50**(6), 889–906.
- Ebert, E. E. and J. A. Curry, 1992: A parameterization of ice cloud optical properties for climate models. *J. Geophys. Res.*, **97**(D4), 3831–3836.
- Ellingson, R. G., J. Ellis and S. Fels, 1991: The intercomparison of radiation codes used in climate models: Longwave results. *J. Geophys. Res.*, **96**(D5), 8929–8953.
- Feingold, G. and A. J. Heymsfield, 1992: Parameterizations of condensational growth of droplets for use in general circulation models. *J. Atmos. Sci.*, **49**(23), 2325–2342.
- Flatau, P. J., G. J. Tripoli, J. Verlinde and W. R. Cotton, 1989: *The CSU-RAMS Cloud Microphysics Module: General Theory and Code Documentation*. Dept. of Atmospheric Science Paper No. 451. Colorado State University, Fort Collins, Colo.
- Fowler, L. D. and D. A. Randall, 1996: Liquid and ice cloud microphysics in the CSU general circulation model. part III: Sensitivity to modeling assumptions. *J. Clim.*, **9**(3), 561–586.
- Fu, R., A. D. Del Genio and W. B. Rossow, 1990: Behavior of deep convective clouds in the tropical pacific deduced from ISCCP radiances. *J. Clim.*, **3**, 1129–1152.
- Gallus, Jr., W. A. and R. H. Johnson, 1991: Heat and moisture budgets of an intense midlatitude squall line. *J. Atmos. Sci.*, **48**(1), 122–146.
- Gamache, J. F. and R. A. Houze, Jr., 1983: Water budget of a mesoscale convective system in the tropics. *J. Atmos. Sci.*, **40**, 1835–1850.
- Grabowski, W. W., M. W. Moncrieff and J. T. Kiehl, 1995: Long-term behavior of precipitating tropical cloud systems: A numerical study. Submitted to *Q. J. R. Meteorol. Soc.*
- Hack, J. J., 1994: Parameterization of moist convection in the National Center for Atmospheric Research community climate model (CCM2). *J. Geophys. Res.*, **99**(D3), 5551–5568.
- Hack, J. J., B. A. Boville, B. P. Briegleb, J. T. Kiehl, P. J. Rasch and D. L. Williamson, 1993: *Description of NCAR community climate model (CCM2)*. NCAR Tech. Note NCAR/TN-382+STR. National Center for Atmospheric Research, Boulder, Colo.
- Hansen, J., G. Russell, D. Rind, P. Stone, A. Lacis, S. Lebedeff, R. Ruedy and L. Travis, 1983: Efficient three-dimensional global models for climate studies: Models I and II. *Mon. Weather Rev.*, **111**(4), 609–662.
- Heymsfield, A., 1972: Ice crystal terminal velocities. *J. Atmos. Sci.*, **29**, 1348–1357.
- Heymsfield, A. J., 1977: Precipitation development in stratiform ice clouds: A microphysical and dynamical study. *J. Atmos. Sci.*, **34**, 367–381.
- Heymsfield, A. J. and L. J. Donner, 1990: A scheme for parameterizing ice cloud water content in general circulation models. *J. Atmos. Sci.*, **47**(15), 1865–1877.
- Heymsfield, A. J. and C. M. R. Platt, 1984: A parameterization of the particle size spectrum of ice clouds in terms of the ambient temperature and the ice water content. *J. Atmos. Sci.*, **41**(5), 846–855.
- Kiehl, J. T., 1994a: On the observed near cancellation between longwave and shortwave cloud forcing in tropical regions. *J. Clim.*, **7**, 559–565.
- Kiehl, J. T., 1994b: Sensitivity of the simulated climate to cloud effective drop size specification. *J. Geophys. Res.*, **99**(D11), 23107–23115.
- Kiehl, J. T., B. A. Boville, B. P. Briegleb, J. J. Hack, P. J. Rasch and D. L. Williamson, 1996: Description of NCAR community climate model (CCM3). Tech. Rep. NCAR/TN-420+STR, National Center for Atmospheric Research, Boulder, Colo.
- Knollenberg, R. G., K. Kelly and J. C. Wilson, 1993: Measurements of high number densities of ice crystals in the tops of tropical cumulonimbus. *J. Geophys. Res.*, **98**(D5), 8639–8664.

- Leary, C. A. and R. A. Houze, Jr., 1980: The contribution of mesoscale motions to the mass and heat fluxes of an intense tropical convective system. *J. Atmos. Sci.*, **37**, 784–796.
- Mahowald, N. M., P. J. Rasch and R. G. Prinn, 1995: Cumulus parameterizations in chemical transport models. *J. Geophys. Res.*, **100**(D12), 26173–26189.
- Ramanathan, V., R. D. Cess, E. F. Harrison, P. Minnis, B. R. Barkstrom, E. Ahmad and D. Hartmann, 1989: Cloud-radiative forcing and climate: Results from the earth radiation budget experiment. *Science*, **243**, 57–63.
- Ramaswamy, V. and A. Detwiler, 1986: Interdependence of radiation and microphysics in cirrus clouds. *J. Atmos. Sci.*, **43**(21), 2289–2301.
- Randall, D. A., Harshvardhan, D. A. Dazlich and T. G. Corsetti, 1989: Interactions among radiation, convection, and large-scale dynamics in a general circulation model. *J. Atmos. Sci.*, **46**(13), 1943–1970.
- Senior, C. A. and J. F. B. Mitchell, 1993: Carbon dioxide and climate: The impact of cloud parameterization. *J. Clim.*, **6**, 393–418.
- Sherwood, S. C., V. Ramanathan, T. P. Barnett, M. K. Tyree and E. Roeckner, 1994: Response of an atmospheric general circulation model to radiative forcing of tropical clouds. *J. Geophys. Res.*, **99**(D10), 20829–20845.
- Slingo, A. and J. M. Slingo, 1988: The response of a general circulation model to cloud longwave radiative forcing. I: Introduction and initial experiments. *Q. J. R. Meteorol. Soc.*, **114**, 1027–1062.
- Slingo, J. M., 1987: The development and verification of a cloud prediction scheme for the ECMWF model. *Q. J. R. Meteorol. Soc.*, **113**, 899–927.
- Smith, R. N. B., 1990: A scheme for predicting layer clouds and their water content in a general circulation model. *Q. J. R. Meteorol. Soc.*, **116**, 435–460.
- Sui, C. H., K. M. Lau, W. K. Tao and J. Simpson, 1994: The tropical water and energy cycles in a cumulus ensemble model. part I: Equilibrium climate. *J. Atmos. Sci.*, **51**(5), 711–728.
- Sun, D.-Z. and R. S. Lindzen, 1993: Distribution of tropical tropospheric water vapor. *J. Atmos. Sci.*, **50**(12), 1643–1660.
- Sundqvist, H., 1988: Parameterization of condensation and associated clouds in models for weather prediction and general circulation simulation. in M. C. Schlesinger, editor, *Physically-Based Modelling and Simulation of Climate and Climatic Change—Part I*, pp. 433–461. Kluwer.
- Tiedtke, M., 1993: Representation of clouds in large-scale models. *Mon. Weather Rev.*, **121**, 3040–3061.
- Tripoli, G. J., 1992: A nonhydrostatic mesoscale model designed to simulate scale interaction. *Mon. Weather Rev.*, **120**, 1342–1359.
- Warren, S. G., C. J. Hahn, J. London, R. M. Chervin and R. L. Jenne, 1986: *Global Distribution of Total Cloud Cover and Cloud Type Amounts Over Land*. NCAR Tech. Note NCAR/TN-273+STR. National Center for Atmospheric Research, Boulder, Colo., NTIS PB87-006903/AS.
- Warren, S. G., C. J. Hahn, J. London, R. M. Chervin and R. L. Jenne, 1988: *Global Distribution of Total Cloud Cover and Cloud Type Amounts over the Ocean*. NCAR Tech. Note NCAR/TN-317+STR. National Center for Atmospheric Research, Boulder, Colo., NTIS DE90-003187.
- Washington, W. M. and C. L. Parkinson, 1986: *An Introduction to Three-Dimensional Climate Modeling*. University Science Books, Mill Valley, CA.
- Wong, T., G. L. Stephens, W. Paul Stackhouse, Jr. and F. P. J. Valero, 1993a: The radiative budgets of a tropical mesoscale convective system during the EMEX-STEP-AMEX experiment 1. observations. *J. Geophys. Res.*, **98**(D5), 8683–8693.
- Wong, T., G. L. Stephens, W. Paul Stackhouse, Jr. and F. P. J. Valero, 1993b: The radiative budgets of a tropical mesoscale convective system during the EMEX-STEP-AMEX experiment 2. model results. *J. Geophys. Res.*, **98**(D5), 8695–8711.
- Xu, K.-M. and S. K. Krueger, 1991: Evaluation of cloudiness parameterizations using a cumulus ensemble model. *Mon. Weather Rev.*, **119**, 342–367.
- Yanai, M., S. Esbensen and J.-H. Chu, 1973: Determination of bulk properties of tropical cloud clusters from large-scale heat and moisture budgets. *J. Atmos. Sci.*, **30**, 611–627.

Zender, C. S. and J. T. Kiehl, 1994: Radiative sensitivities of tropical anvils to small ice crystals. *J. Geophys. Res.*, **99**(D12), 25869–25880.

Zender, C. S. and J. T. Kiehl, 1996: Sensitivity of a climate simulation to representation of tropical anvil. Submitted to *J. Clim.*.

Zhang, G. J. and N. A. McFarlane, 1995: Sensitivity of climate simulations to the parameterization of

cumulus convection in the canadian climate centre general circulation model. *Atmos. Ocean*, **33**(3), 407–446.

This preprint was prepared with the AGU L^AT_EX macros v3.1. File anv'cem formatted 1996 July 19.

With the extension package 'AGU++', version 1.3 from 1995/12/01